Reduced optical loss in mechanically stacked multi-junction organic solar cells exhibiting complementary absorptions

Yen-Tseng Lin,[1] Chu-Hsien Chou,[2] Fang-Chung Chen,[2,*] Chih-Wei Chu,[3] and Chain-Shu Hsu[4]

[1] *Institute of Lighting and Energy Photonics, National Chiao Tung University, 301 Gaofa 3rd Road, Tainan 71150, Taiwan*

[2] *Department of Photonics, National Chiao Tung University, 1001 University Road, Hsinchu 30010, Taiwan*

[3] *Research Center of Applied Science, Academia Sinica, Taipei 115, Taiwan*

[4] *Department of Applied Chemistry, National Chiao Tung University, 1001 University Road, Hsinchu 30010, Taiwan*

[*] *fcchen@mail.nctu.edu.tw*

Abstract: This paper describes a promising approach toward preparing effective electrical and optical interconnections for tandem organic photovoltaic devices (OPVs). The first subcell featured a semi-transparent electrode, which allowed a portion of the solar irradiation to pass through and to enter the second subcell exhibiting complementary absorption behavior. The resulting multi-junction OPV had multiple contacts such that the subcells could be easily connected either in series or in parallel. More importantly, we used UV-curable epoxy to "mechanically" stack the two subcells and to eliminate the air gap between them, thereby reducing the optical loss induced by mismatches of refractive indices. Therefore, an improved power conversion efficiency of approximately 6.5% has been achieved.

OCIS codes: (040.5350) Photovoltaic; (160.4890) Organic materials; (350.6050) Solar energy.

References and links

1. M. A. Green, K. Emery, Y. Hishikawa, W. Warta, and E. D. Dunlop, "Solar cell efficiency tables (version 39)," Prog. Photovolt. Res. Appl. **20**(1), 12–20 (2012).
2. W. Shockley and H. J. Queisser, "Detailed balance limit of efficiency of *p-n* junction solar cells," J. Appl. Phys. **32**(3), 510–519 (1961).
3. G. F. Brown and J. Wu, "Third generation photovoltaics," Laser Photon. Rev. **3**(4), 394–405 (2009).
4. A. De Vos, "Detailed balance limit of the efficiency of tandem solar cells," J. Phys. D Appl. Phys. **13**(5), 839–846 (1980).
5. D. Shahrjerdi, S. W. Bedell, C. Ebert, C. Bayram, B. Hekmatshoar, K. Fogel, P. Lauro, M. Gaynes, T. Gokmen, J. A. Ott, and D. K. Sadana, "High-efficiency thin-film InGaP/InGaAs/Ge tandem solar cells enabled by controlled spalling technology," Appl. Phys. Lett. **100**(5), 053901 (2012).
6. G. Li, R. Zhu, and Y. Yang, "Polymer solar cells," Nat. Photonics **6**(3), 153–161 (2012).
7. H. L. Yip and A. K.-Y. Jen, "Recent advances in solution-processed interfacial materials for efficient and stable polymer solar cells," Energy Environ. Sci. **5**(3), 5994–6011 (2012).
8. J. L. Wu, F. C. Chen, Y. S. Hsiao, F. C. Chien, P. Chen, C. H. Kuo, M. H. Huang, and C. S. Hsu, "Surface plasmonic effects of metallic nanoparticles on the performance of polymer bulk heterojunction solar cells," ACS Nano **5**(2), 959–967 (2011).
9. A. L. Roes, E. A. Alsema, K. Blok, and M. K. Patel, "Ex-ante environmental and economic evaluation of polymer photovoltaics," Prog. Photovolt. Res. Appl. **17**(6), 372–393 (2009).
10. A. Kumar, R. Devine, C. Mayberry, B. Lei, G. Li, and Y. Yang, "Origin of radiation-induced degradation in polymer solar cells," Adv. Funct. Mater. **20**(16), 2729–2736 (2010).
11. J. L. Wu, F. C. Chen, M. K. Chuang, and K. S. Tan, "Near-infrared laser-driven polymer photovoltaic devices and their biomedical applications," Energy Environ. Sci. **4**(9), 3374–3378 (2011).
12. G. Dennler, M. C. Scharber, T. Ameri, P. Denk, K. Forberich, C. Waldauf, and C. J. Brabec, "Design rules for donors in bulk-heterojunction tandem solar cells-towards 15% energy-conversion efficiency," Adv. Mater. **20**(3), 579–583 (2008).

#204965 - $15.00 USD Received 17 Jan 2014; revised 13 Feb 2014; accepted 15 Feb 2014; published 25 Feb 2014

13. S. Sista, X. Hong, L. M. Chen, and Y. Yang, "Tandem polymer photovoltaic cells—current status, challenges and future outlook," Energy Environ. Sci. **4**(5), 1606–1620 (2011).
14. L. Dou, J. You, J. Yang, C. C. Chen, Y. He, S. Murase, T. Moriarty, K. Emery, G. Li, and Y. Yang, "Tandem polymer solar cells featuring a spectrally matched low-bandgap polymer," Nat. Photonics **6**(3), 180–185 (2012).
15. J. You, L. Dou, K. Yoshimura, T. Kato, K. Ohya, T. Moriarty, K. Emery, C. C. Chen, J. Gao, G. Li, and Y. Yang, "A polymer tandem solar cell with 10.6% power conversion efficiency," Nat Commun **4**, 1446 (2013).
16. M. Riede, C. Uhrich, J. Widmer, R. Timmreck, D. Wynands, G. Schwartz, W. Gnehr, D. Hildebrandt, A. Weiss, J. Hwang, S. Sundarraj, P. Erk, M. Pfeiffer, and K. Leo, "Efficient organic tandem solar cells based on small molecules," Adv. Funct. Mater. **21**(16), 3019–3028 (2011).
17. F. C. Chen and C. H. Lin, "Construction and characteristics of tandem organic solar cells featuring small molecule-based films on polymer-based subcells," J. Phys. D Appl. Phys. **43**(2), 025104 (2010).
18. W. C. Chen, S. C. Chien, F. C. Chen, and C. S. Hsu, "Stacked structures for assembling multiple organic photovoltaic devices," Appl. Phys. Express **5**(7), 072301 (2012).
19. V. Shrotriya, E. H. E. Wu, G. Li, Y. Yao, and Y. Yang, "Efficient light harvesting in multiple-device stacked structure for polymer solar cells," Appl. Phys. Lett. **88**(6), 064104 (2006).
20. R. F. Bailey-Salzman, B. P. Rand, and S. R. Forrest, "Semitransparent organic photovoltaic cells," Appl. Phys. Lett. **88**(23), 233502 (2006).
21. Z. Tang, Z. George, Z. Ma, J. Bergqvist, K. Tvingstedt, K. Vandewal, E. Wang, L. M. Andersson, M. R. Andersson, F. Zhang, and O. Inganäs, "Semi-transparent tandem organic solar cells with 90% internal quantum efficiency," Adv. Energy Mat. **2**(12), 1467–1476 (2012).
22. W. T. Lin, Y. T. Lin, C. H. Chou, F. C. Chen, and C. S. Hsu, "Organic solar cells comprising multiple-device stacked structures exhibiting complementary absorption behavior," Sol. Energy Mater. Sol. Cells **120**, 724–727 (2014).
23. Y. J. He, H. Y. Chen, J. H. Hou, and Y. F. Li, "Indene-C_{60} bisadduct: a new acceptor for high-performance polymer solar cells," J. Am. Chem. Soc. **132**(4), 1377–1382 (2010).
24. M. A. Ibrahem, H. Y. Wei, M. H. Tsai, K. C. Ho, J. J. Shyue, and C. W. Chu, "Solution-processed zinc oxide nanoparticles as interlayer materials for inverted organic solar cells," Sol. Energy Mater. Sol. Cells **108**, 156–163 (2013).
25. J. K. Lee, W. L. Ma, C. J. Brabec, J. Yuen, J. S. Moon, J. Y. Kim, K. Lee, G. C. Bazan, and A. J. Heeger, "Processing additives for improved efficiency from bulk heterojunction solar cells," J. Am. Chem. Soc. **130**(11), 3619–3623 (2008).
26. F. C. Chen, H. C. Tseng, and C. J. Ko, "Solvent mixtures for improving device efficiency of polymer photovoltaic devices," Appl. Phys. Lett. **92**(10), 103316 (2008).
27. G. Li, Y. Yao, H. Yang, V. Shrotriya, G. Yang, and Y. Yang, ""Solvent annealing" effect in polymer solar cells based on poly(3-hexylthiophene) and methanofullerenes," Adv. Funct. Mater. **17**(10), 1636–1644 (2007).
28. F. C. Chen, C. J. Ko, J. L. Wu, and W. C. Chen, "Morphological study of P3HT:PCBM blend films prepared through solvent annealing for solar cell applications," Sol. Energy Mater. Sol. Cells **94**(12), 2426–2430 (2010).
29. V. Shrotriya, G. Li, Y. Yao, T. Moriarty, K. Emery, and Y. Yang, "Accurate measurement and characterization of organic solar cells," Adv. Funct. Mater. **16**(15), 2016–2023 (2006).
30. L. J. Huo, S. Q. Zhang, X. Guo, F. Xu, Y. F. Li, and J. H. Hou, "Replacing alkoxy groups with alkythienyl groups: A fesible approach to improve the properties of photovoltaic polymers," Angew. Chem. Int. Ed. **50**(41), 9697–9702 (2011).
31. Y. Yao, H. Y. Chen, J. Huang, and Y. Yang, "Low voltage and fast speed all-polymeric optocouplers," Appl. Phys. Lett. **90**(5), 053509 (2007).
32. C. H. Chou, J. K. Chuang, and F. C. Chen, "High-performance flexible waveguiding photovoltaics," Sci. Rep. **3**, 2244 (2013).

1. Introduction

Solar energy is by far the most abundant, sustainable and long-term energy resource, in contrast to traditional energy supplies such as coal and fossil fuels. One direct method of converting solar radiation to electricity makes use of photovoltaic (PV) devices. Currently, single-junction PV cells have been reported to achieve power conversion efficiencies (PCEs) of up to 30% [1]. Thermodynamics, however, limits the PCEs fundamentally, which is known as Shockley-Queisser or the detailed balance limit [2]. In order to increase the efficiencies beyond the limit, many approaches have been proposed [3]. For example, harvesting hot carriers or incorporating intermediate-bands, has been shown to be effective for improving the cell efficiencies. Among these techniques, De Vos demonstrated that stacking multiple subcells allows theoretical PCEs to surpass the Shockley–Queisser limit because the electrochemical potential of charge carrier extraction is increased [4]. Therefore, a staggering amount of research has been conducted in the development of multi-junction PV devices [3,5].

#204965 - $15.00 USD Received 17 Jan 2014; revised 13 Feb 2014; accepted 15 Feb 2014; published 25 Feb 2014

Organic photovoltaic devices (OPVs) hold great promise for next-generation solar cells because of their advantageous properties including inexpensive fabrication, mechanical flexibility, light weight and short energy pay-back times [6–9]. The unique material properties of OPVs enable a wide range of potential applications, including energy resources for outer space and biomedical treatments [10,11]. However, further efforts will be still required to improve their efficiencies for practical applications. One of the key issues toward high efficiencies is sufficient photon absorption. The thickness of the photoactive layer in typical OPVs, however, is limited at approximately 100 nm, meaning that it cannot absorb all of the incident photons, due to the low mobility of organic materials and the high degree of charge recombination. In other words, the use of a thicker photoactive layer for harvesting more photons is severely restricted. Furthermore, the absorption range of single organic materials is usually narrow, thereby limiting the use of the full spectrum range of the solar irradiation. One effective approach for solving these problems is to produce multi-junction cells [12–17]. Theoretically, the PCE of multi-junction OPVs could be achieved as high as 15% [12]. The PCE of state-of-art tandem OPVs is over 10% [15].

There are generally two methods for stacking multiple cells [3]. The most common one is to integrate the subcells monolithically with tunnel junctions. The cells are naturally connected in series and only two terminals exist in this typical of design. The other method is to connect the physically separated subcells using multiple connects; this structure removes the current restriction and the subcells can be connected either in series or in parallel. For OPVs, most research of tandem cells carried out has focus on the development of two-terminal tandem cells [12,13]. Nevertheless, the fabrication of multi-junction OPVs usually involves sophisticated procedures. The device fabrication yield usually becomes lower due to the complicated device structures, especially for solution-processed tandem structures [18]. Previously, Shrotriya *et al*. reported an alternative method for fabricating multi-junction devices: they first developed a semitransparent (ST) subcell and superimposed it onto another conventional one with a standard device structure [19]. Such multi-junction device could be connected either in series or in parallel. The PCE of the device comprising the so-called multiple-device stacked structure could be doubled relative to the efficiency of the corresponding single-junction device [19]. Nevertheless, most multiple-device stacked structures reported so far have utilized identical material systems in the subcells, resulting in limited absorption range [18–20]. OPVs comprising physically separated subcells exhibiting complementary absorptions are still very rare [21,22]. Moreover, the optics in the tandem OPVs is still not well understood yet.

Herein, we describe a new method for constructing tandem structures through stacking of two subcells exhibiting complementary absorption behavior. The multi-junction OPV featured multiple contacts for each subcell; they could be easily connected either in series or in parallel. Therefore, no current matching restriction was imposed while they were joined in parallel. More importantly, we used UV-curable epoxy to “mechanically” stack the two subcells and to eliminate the air gap between them. The epoxy layer reduced the optical loss induced by the mismatch of refractive indices in the structures. As a result, an improved PCE of approximately 6.5% under illumination at one sun has been achieved.

2. Experimental

The chemical structures of the materials used in this work are illustrated in Fig. 1. The low-band-gap (LBG) polymer and the fullerene derivatives of the photoactive layer in the front subcell were poly{[4,8-bis-(2-ethyl-hexyl-thiophene-5-yl)-benzo[1,2-b:4,5-b’]dithiophene-2,6-diyl]-*alt*-[2-(2’-ethyl-hexanoyl)-thieno[3,4-b]thiophen-4,6-diyl]} (PBDTTT-C-T) and [6,6]-phenyl-C-61-butyric acid methyl ester ($PC_{60}BM$), respectively. In the rear subcell, the donor polymer was poly(3-hexylthiophene) (P3HT); the acceptor was replaced by Indene-C_{60} bisadduct ($IC_{60}BA$), another C_{60} derivative that possesses a higher lowest unoccupied molecular orbital (LUMO) [23], to improve the open-circuit voltage. Figure 1 also illustrates

#204965 - $15.00 USD Received 17 Jan 2014; revised 13 Feb 2014; accepted 15 Feb 2014; published 25 Feb 2014

the device structure of the multi-junction OPVs in this work. The front subcell consisted of a ST Ag electrode, which allowed a portion of the solar irradiation to pass though the device and to enter the rear subcell. To fabricate the ST device, a solution of zinc oxide (ZnO) nanoparticles dissolved in ethylene glycol (EG) was spin-coated onto an indium tin oxide (ITO)-coated glass substrate and the sample was baked at 150°C for 1 h [24]. Then, a solution of PBDTTT-C-T/$PC_{60}BM$ blend in 1,2-dicholorobenzene (DCB) were further coated onto the substrate. Note that 3 vol.% of 1,8-diiodooctane was used as the additive during the sample preparation [25,26]. Next, MoO_3 (3.5 nm) and Ag (15 nm) were deposited to form the ST electrodes [18,22]. Because of the long skin depth and high electrical conductivity, we chose Ag as the electrode material and the thickness has been optimized according to our previous works [18,22]. For the fabrication of the rear subcell devices, poly(3.4-ethylenedioxythiophe):poly(styrene sulfonate) (PEDOT:PSS) was deposited on the ITO-coated glass substrate and the resulting film was baked at 120°C for 1 h. Next, P3HT:$IC_{60}BA$ blends dissolved in DCB were further coated onto top of the PEDOT:PSS layer. After the solvent annealing process [27,28], the sample was further thermally annealed at 150°C for 10 min. Then, Ca (30nm) and Al (100 nm) were deposited through thermal evaporation. Finally, we used UV curable epoxy (EPOXY Technology) and cover glasses to package the devices. Current density-voltage *(J-V)* characteristics of the OPVs were measured using the Keithley 2400 source measurement system; the photocurrent densities were obtained while the devices were illuminated with a 150 W Thermal Oriel solar simulator. The illumination intensity was calibrated using a Si photodiode equipped with a KG-5 filter (Hamamatsu, Inc.) [29]. The external quantum efficiency (EQE) spectra were obtained using an EQE measurement system (Enli Technology). The absorption spectra were recorded using a Perkin-Elmer Lambda 650 ultraviolet/visible/near infrared spectrometer.

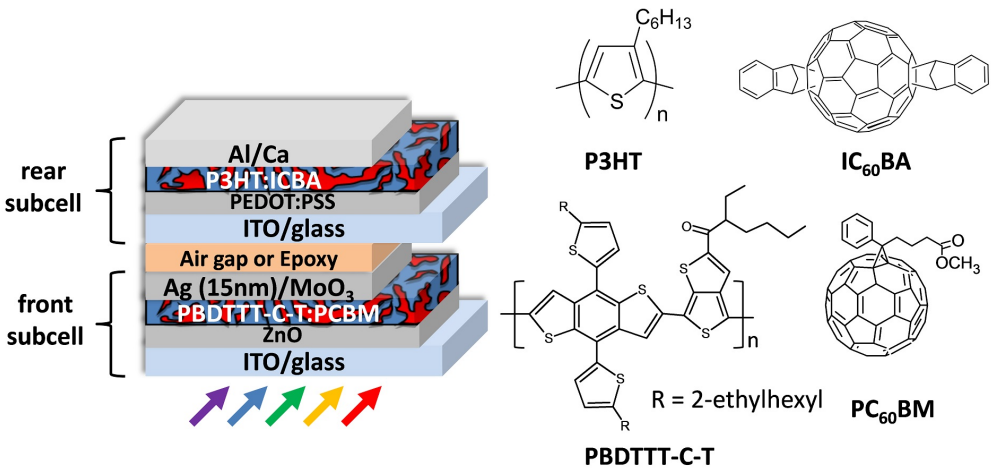

Fig. 1. (a) Schematic representation of the device structure of the multi-junction OPVs. (b) Chemical structures of the materials (PBDTTT-C-T, P3HT, $PC_{60}BM$ and $IC_{60}BA$) used in this work.

3. Result and discussions

Figure 2(a) shows that the absorption spectra of the photoacive layers in the subcells. The major absorption of the P3HT:$IC_{60}BA$ thin film in the rear subcell was located between 400 and 600 nm. On the other hand, the PBDTTT-C-T:$PC_{60}BM$ layer featured the major absorption between 600 and 800 nm. Indeed, the absorption onset of PBDTTT-C-T is located at 784 nm, suggesting a low bandgap at 1.58 eV [30]. Apparently, the absorption of the multi-junction OPVs consisting of the two material systems covered the solar spectrum over the range from 400 to 800 nm in a complementary manner.

#204965 - $15.00 USD Received 17 Jan 2014; revised 13 Feb 2014; accepted 15 Feb 2014; published 25 Feb 2014

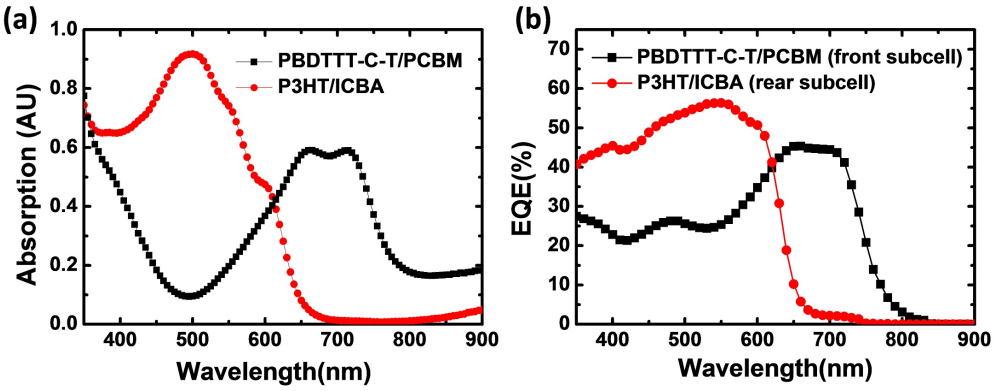

Fig. 2. (a) Absorption spectra of the films of PBDTTT-C-T:$PC_{60}BM$ film (1:1.5, w/w) and the P3HT:$IC_{60}BA$ (1:1, w/w). (b) The EQE spectra of the two subcells in the tandem OPVs. The device structures of the front cell and the back cell device are ITO/ZnO(40nm)/PBDTTT-C-T:$PC_{60}BM$ (95 nm)/MoO_3(3.5 nm)/Ag(15nm) and ITO/PEDOT:PSS(45nm)/P3HT:$IC_{60}BA$ (200 nm)/Ca(30nm)/Al(100nm), respectively.

In order to obtain highly efficient tandem OPVs, we firstly investigated the device performance of individual subcells. For the front ST subcell, we adopted an inverted structure, in which the anode comprised a MoO_3/Ag bilayer [22]. Figure 3 displays the transmittance spectrum of the MoO_3/Ag electrode. We could see that the average transmittance was larger than *ca*. 35%, suggesting a reasonable portion of the photons could pass through the semitransparent anode. Figure 3 also presents the overall transmittance spectrum of the ST front subcell. The transmittance values decreased significantly within the spectral range from 550 to 800 nm due to the absorption of the PBDTTT-C-T:$PC_{60}BM$ active layer. On the other hand, within the wavelength range from 400 to 600 nm, which is corresponding to the absorption band of the rear subcell, sufficient transmittance could be still obtained.

The optimized weight ratio of PBDTTT-C-T to $PC_{60}BM$ was found to be 1:1.5 in the front subcell. The best thickness of the photoactive layer was ~100 nm [22]. Figure 4(a) shows the *J–V* curve for the optimized front subcell obtained under standard illumination condition (AM 1.5G, 100 mW cm^{-2}). The device exhibited an open-circuit voltage (V_{oc}) of 0.77 V, a short-current (J_{sc}) of 10.39 mA cm^{-2}, and a fill factor (FF) of 0.53, resulting in a PCE of 4.27%. Figure 4(a) also displays the *J–V* curve of the rear subcell. As expected, the photovoltage was increased to 0.83 V, which was larger than that of a typical P3HT:$PC_{60}BM$-based device (i.e., 0.59V) [11], due to the higher LUMO energy of ICBA [23]. Further, The values of J_{sc} and FF were 10.21 mA cm^{-2}, and 0.62, respectively; the calculated PCE was 5.24%.

Figure 2(b) presents the EQE spectra of the individual subcells. We could clearly see that the front subcell had broad response ranges covering 350-800 nm. The major photoresponse range, however, was from 600 to 800 nm. The maximum EQE was 45% at 650 nm. On the other hand, the rear subcell exhibited wavelength response range covering 350-650 nm. The EQE peak reached 59% at 550 nm. Overall, the results of EQE spectra were consistence with the conclusion draw from the absorption spectra [Fig. 2(a)] and confirmed the complementary behavior of absorption for these two subcells.

#204965 - $15.00 USD Received 17 Jan 2014; revised 13 Feb 2014; accepted 15 Feb 2014; published 25 Feb 2014

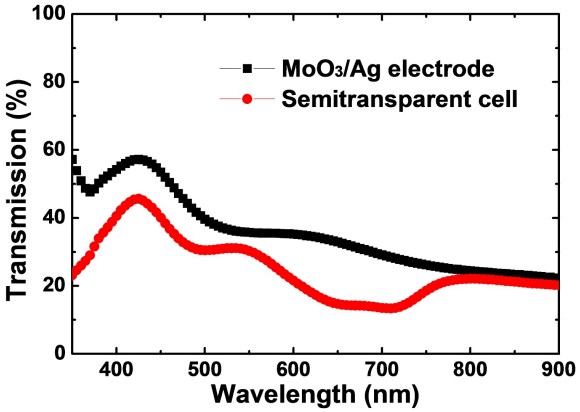

Fig. 3. The transmittance spectra of the front subcell and its semitransparent anode. Device structure: ITO/ZnO(40nm)/PBDTTT-C-T:$PC_{60}BM$ (95 nm)/MoO_3(3.5 nm)/Ag(15nm).

Next, we constructed multi-junction OPVs by connecting the two subcells either in parallel or in series [Fig. 1(a)]. Because the structure had 4 terminals, the *J-V* characteristics of the individual subcells and of the tandem OPVs could be obtained simultaneously; Fig. 4(a) shows the results. During the testing period, which was typical less than an hour, no degradation was observed. From the *J-V* curves, we can see that the rear subcell exhibited a lower photocurrent (i.e., 4.96 mA cm^{-2}) than that of the subcell measured before connection with the front subcell. This was due to the fact that a portion of the solar irradiation was absorbed and/or blocked by the front subcell. We also noted that the FF remained the same but the V_{oc} was slightly reduced to 0.81V, resulting in a PCE of 2.49%. When the subcells were connected in series, the multi-junction OPV exhibited a PCE of 5.37% with a V_{oc} of 1.57 V, J_{sc} of 5.53 mA cm^{-2}, FF of 0.62. The V_{oc} is very close to the sum of the photovotages of the two isolated subcells (0.77 for the front subcell and 0.81V for the rear subcell), suggesting the electrical connection was effective. However, the J_{sc} was apparently limited by the rear subcell because the current in the same loop should be identical according to the Kirchhoff's law. As a result, the PCE of the tandem structure with series connection was only slightly higher than that of the isolated rear subcell (i.e., 5.24%). On the other hand, when we connected the subcells in parallel, the tandem OPV exhibited a much better performance with V_{oc}, J_{sc}, and FF values of 0.77 V, 15.70 mA cm^{-2}, and 0.51, respectively; the calculated PCE was 6.18%. The photocurrent clearly was not limited by the current matching. Its value was very close to the sum of the photocurrent of the subcells measured individually in the tandem configuration (i.e., 10.39 mA cm^{-2} for the front subcell and 4.96 mA cm^{-2} for the rear subcell). Subsequently, the value of the PCE was also close to the sum of the PCEs of the subcells measured individually in the tandem configuration (i.e., 4.27% for the front subcell and 2.49% for the rear subcell). These results suggest that very limited power loss occurred and the power of the two subcells could be drawn separately in this multi-junction OPV. More importantly, the improved PCE was higher than that of both isolated subcells measured under standard illumination condition at 1 sun (i.e., 4.27% for the front subcell and 5.24% for the rear subcell). Table 1 summarizes the detailed device parameters of the isolated subcells and the multi-junction OPV.

#204965 - $15.00 USD Received 17 Jan 2014; revised 13 Feb 2014; accepted 15 Feb 2014; published 25 Feb 2014

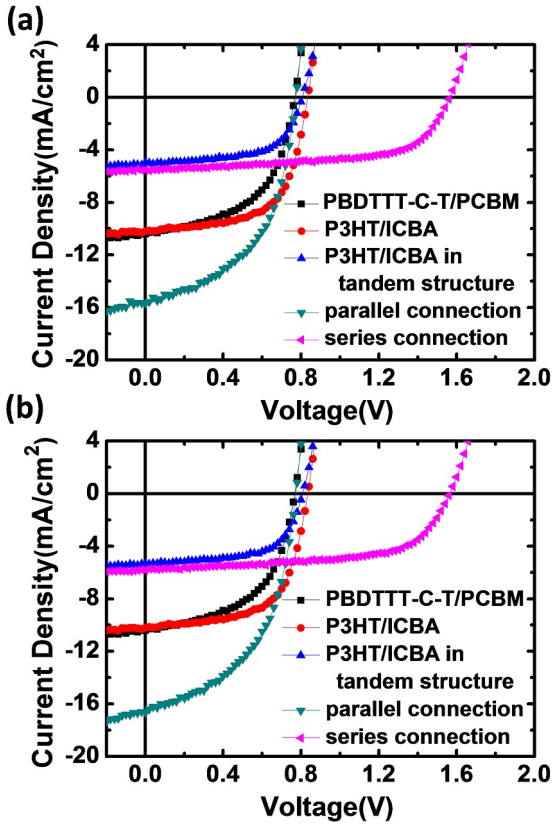

Fig. 4. *J-V* curves of the front ST subcells, the rear subcells, and the tandem OPV connected either in series or in parallel measured under AM 1.5G illumination (100 mW cm^{-2}). (a) An air gap was present between the subcells; (b) a layer of UV curable epoxy was inserted between the subcells.

Table 1. Photovoltaic parameters of individual subcells and tandem structures. An air gap existed between the subcells in the tandem cells.

Device condition	V_{oc} (V)	J_{sc} (mA cm^{-2})	FF	PCE (%)
Front cell[a]	0.77	10.39	0.53	4.27
Rear cell[a]	0.83	10.21	0.62	5.24
Front cell in tandem structure	0.77	10.39	0.53	4.27
Rear cell in tandem structure	0.81	4.96	0.62	2.49
Tandem (connected in series)	1.57	5.53	0.62	5.37
Tandem (connected in parallel)	0.77	15.70	0.51	6.18

[a]The device was not connected to another subcell; it was measured individually.

When we carefully examined the structure the multi-junction device, we could find that an air gap existed between the two subcells, resulting in mismatches of refractive indices. The refractive indexes of the glass substrate and the top cover glass for encapsulation were both 1.460, resulting in a typical refraction-index profile of n-1-n structure. To simplify the problem in the beginning, we used the following formula to calculate the transmittance (T),

$$T = \frac{4n_1 n_2}{(n_1 + n_2)^2} \quad (1)$$

where n_1 and n_2 were the refractive indexes of glass and air, respectively. The T value was calculated as 96.50% across the glass/air interface. In the tandem OPV, because there were

#204965 - $15.00 USD Received 17 Jan 2014; revised 13 Feb 2014; accepted 15 Feb 2014; published 25 Feb 2014

two distinctive interfaces, we obtained a transmittance value (T^2) of 93.13%. Obviously, significant optical loss (approximately 7%) occurred in the tandem structure due to the mismatches of refractive index. In order to reduce the optical loss, we used UV curable epoxy (n = 1.519) to fill the air gap. Following Eq. (1) and assuming that n_1(glass) and n_2(epoxy) were 1.460 and 1.519, respectively, we obtained a transmittance value (T^2) of 99.92%. In other words, we deduced that more than 6% of photon flux could be harvested if the air gap had been filled [31].

Following the above results of calculation, we further used the UV-curable epoxy to "mechanically" stack the two subcells; the electrical characteristics of the resulting tandem cells is displayed in Fig. 4(b). We found that the J_{sc} value of the rear cell increased from 4.96 mA cm^{-2} to 5.29 mA cm^{-2}. While the values of V_{oc} and FF remained unchanged (0.81 V and 0.62, respectively), the larger photocurrent led to an improved PCE of 2.66%. Note that the *ca*. 6.6% enhancement in J_{sc} of the rear subcell was correspondent with the prediction from the above calculation. Because of the reduced optical loss, the tandem OPV connected in series also exhibited a higher photocurrent (i.e., 5.80 mA cm^{-2}). The values of V_{oc} and FF were 1.57 V and 0.61, respectively, resulting a higher PCE of 5.60%. More interestingly, the device connected in parallel exhibited the best performance, with V_{oc}, J_{sc}, and FF values of 0.77 V, 16.64 mA cm^{-2}, and 0.51, respectively; its PCE became 6.47%. The improvement in PCE reflected that such mechanically stacking approach is effective for reducing the optical loss due to the mismatches of refractive indices arose from the air gap [31]. Table 2 summarizes the detailed device parameters of the isolated subcells and the multi-junction OPV after the air gap was eliminated.

Table 2. Photovoltaic parameters of individual subcells and tandem structures. The air gap between the subcells was eliminated with UV-curable epoxy.

Device condition	V_{oc} (V)	J_{sc} (mA cm^{-2})	FF	PCE (%)
Front cell in tandem structure	0.77	10.39	0.53	4.27
Rear cell in tandem structure	0.81	5.29	0.62	2.66
Tandem (connected in series)	1.57	5.80	0.61	5.60
Tandem (connected in parallel)	0.77	16.64	0.51	6.47

Figure 5(a) displays the EQE spectra of the rear cells in the tandem structures before and after the air gap was filled by epoxy. Comparing the results with the spectrum of the individual P3HT:ICBA subcell [Fig. 2(b)], we can see that the rear cells exhibited different spectral response. Because of the absorption of the front cell, the EQE values apparently became lower. Especially, within the overlapping spectral range from 500 to 650 nm, the quantum efficiencies were significantly affected. On the other hand, we also observed that the efficiencies were increased after the air gap was eliminated. For example, the quantum efficiency was increased from 16% to 18% at the peak wavelength of 455 nm. These results further support the optical function of the UV-curable epoxy. Figure 5(b) also illustrates the EQE spectra of the tandem structures connected in parallel. Both spectra exhibited well photocurrent response from 350 to 800 nm, suggesting the complementary absorption manner of photoabsorption of the two subcells [22]. Further, we also calculated the photocurrent values from the EQE spectrum in Fig. 5(b). The photocurrent was originally 15.8 mA cm^{-2} before the air gap was filled. The photocurrent, however, was increased to 16.6 mA cm^{-2} after filling the air gap. The *ca.* 5% enhancement of photocurrent further confirmed the recovery of the optical loss in the mechanically stacked tandem structures.

#204965 - $15.00 USD Received 17 Jan 2014; revised 13 Feb 2014; accepted 15 Feb 2014; published 25 Feb 2014

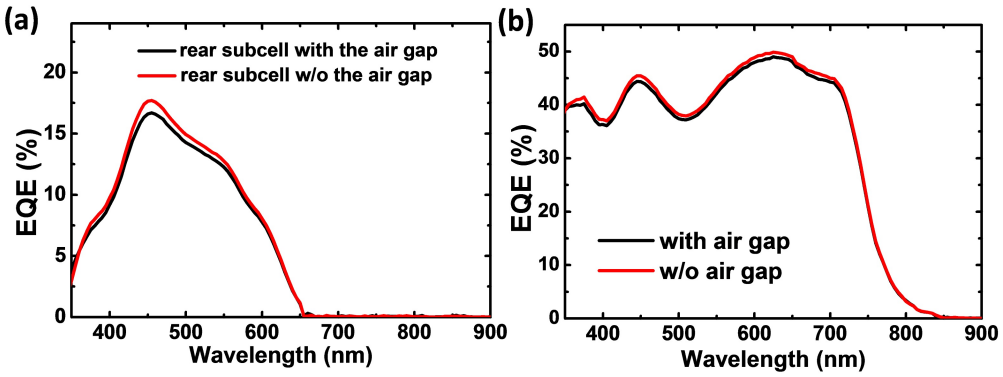

Fig. 5. (a) The EQE spectra of the rear subcells in the tandem OPVs before and after the air gap was filled. (b) The EQE spectra of the tandem cells connected in parallel before and after the air gap was filled.

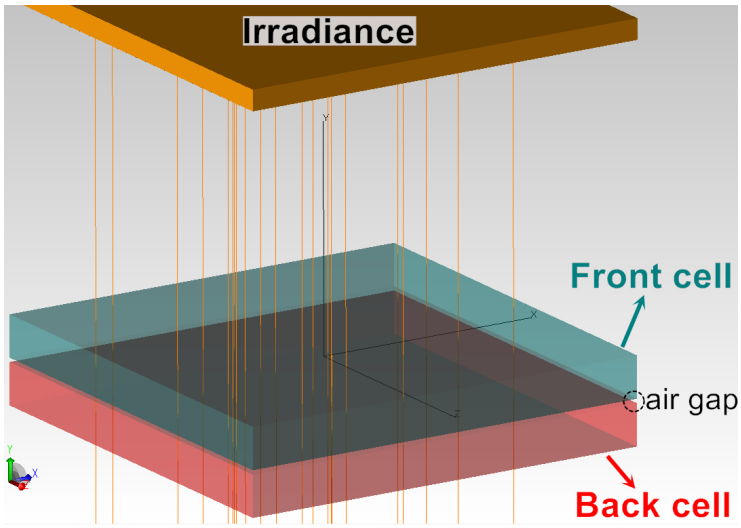

Fig. 6. Imitating the transmittances of the tandem cells in TracePro®. A 1 mm air gap existed between the front and rear subcells; the spectrum of the solar irradiance was set according to IEC 60904-9.

To further confirm the conclusion drawn from the previous section, we used a commercial ray-tracing software, TracePro® (Lambda Research), to simulate the experimental results [32]. In the simulation, we considered the material of both front and rear subcells as glass (n = 1.460) and the size of both devices was 10.0 x 10.0 x 1.0 mm^3. Further, there was a 0.1 mm-thick air gap between the two subcells. Similarly, the refractive indices of air and UV-curable epoxy were simply set as 1.000 and 1.519, respectively. Imitation light, according to IEC 60904-9, was introduced as the light source [32]. The stimulation condition was depicted in Fig. 6. The top surface of the front subcell was set as a transmittance surface and the bottom surface of the rear subcell was set as a perfect absorber. The simulation results indicated that only 89.35% of the photons was absorbed by the bottom surface after passing through the entire structure while the air gap was present. Nevertheless, the value increased to 96.38% when the air gap was eliminated with the epoxy. In short, the simulation confirms *ca.* 7% of optical loss can be recovered after filling the air gap. Overall, the results were consistent with the conclusion of the numerical calculations and the experimental data.

#204965 - $15.00 USD Received 17 Jan 2014; revised 13 Feb 2014; accepted 15 Feb 2014; published 25 Feb 2014

4. Conclusions

We have developed a promising approach for constructing multi-junction OPVs exhibiting complementary absorption behavior. In this design, the first ST subcell adopted an inverted structure and a LBG polymer was used as its photoactive layer. The ST subcell also featured a MoO_3/Ag bilayered anode as the highly transparent top electrode. The second subcell featuring complementary absorption was fabricated with the conventional structure; it was stacked onto the first ST subcells. The resulting multi-junction OPV had four contacts such that they could be easily connected either in series or in parallel. Because the two subcells exhibited complementary absorptions, an improved PCE has been achieved. We also found that the tandem OPV exhibited a higher PCE while the subcells were connected in parallel. The power of the two subcells could be drawn separately in this multi-junction design. More importantly, after a UV curable epoxy was used to mechanically stack the subcells and to eliminate the air gap between them, the reduction of optical loss due to the mismatches of refractive indices at the interfaces increased the device PCE. In short, the epoxy layer exhibited two functions: it "mechanically" connected both subcells and fixed the problem of the mismatches of refractive indices by filling the air gap. Finally, we believe that the device preparation scheme reported herein opens up the opportunity fabricating effective electrical and optical interconnections for tandem OPVs in high yield.

Acknowledgments

We thank the National Science Council of Taiwan (Grant Nos.: NSC 102-3113-P-009-004, NSC 102-2221-E-009-130-MY3, and NSC 101-2628-E-009-008-MY3) and the Ministry of Education of Taiwan (through the ATU program) for financial support.

#204965 - $15.00 USD Received 17 Jan 2014; revised 13 Feb 2014; accepted 15 Feb 2014; published 25 Feb 2014